Properties of the scalar variance transport equation in turbulent channel flow

Ang Zhou* and Joseph Klewicki†
Department of Mechanical Engineering, University of New Hampshire, Durham, New Hampshire 03824, USA

Sergio Pirozzoli‡
Dipartimento di Ingegneria Meccanica e Aerospaziale, Sapienza Università di Roma, Via Eudossiana 18, 00184 Roma, Italy

(Received 15 August 2018; published 15 February 2019)

The asymptotic scaling structure of the total scalar variance equation is investigated for fully developed turbulent channel flow subjected to uniform scalar generation. The total scalar variance balance has a four-layer structure similar to that of the total kinetic energy balance, as previously investigated by Zhou and Klewicki [Phys. Rev. Fluids **1**, 044408 (2016)]. Direct numerical simulation data are used to quantify the leading balance structure. These data cover the friction Reynolds number up to $\delta^+ = 4088$ and Prandtl number ranging between $\mathrm{Pr} = 0.2$ and 1.0. Of the layers empirically characterized, the inner-normalized width of the third layer is analytically verified to be $\delta^+ - \sqrt{\delta^+/\mathrm{Pr}}$. This result agrees closely with the empirical observations. Consistent with previous observations, the Kármán constant, k_θ, for the mean scalar profile for $\mathrm{Pr} = 1$ is shown to be greater than the Kármán constant, k, for the mean velocity profile. Unlike previous studies, the present problem formation yields identical mean equations and boundary conditions for the scalar and velocity, and this allows unambiguous comparisons regarding the noted differences between k and k_θ. Results from the mean transport equations and streamwise velocity and scalar variance budget equations, as well as the relevant correlation coefficient profiles, are used to clarify the source of the differences between k and k_θ. Through the present theory, the results reported herein connect the statistical structure of the scalar and velocity fields to the mean profile slopes.

DOI: 10.1103/PhysRevFluids.4.024606

I. INTRODUCTION

Multiple-scale analysis approaches are often used to better understand wall turbulence at high Reynolds number. Among these, the notion of an overlap layer is prevalent [1,2]. Application of the overlap concept generically involves respective functions of inner and outer normalized distance from the wall, and that these inner and outer descriptions have simultaneous validity over some interior domain. For many laminar flows, the underlying machinery associated with the development of matched asymptotic expansions has a well-founded analytical basis. On the other

*Present address: Center for Magnetic Resonance Research, University of Minnesota, Minneapolis, Minnesota 55455, USA; zhouang48@gmail.com
†Present address: Department of Mechanical Engineering, University of Melbourne, Victoria 3010, Australia; klewicki@unimelb.edu.au
‡sergio.pirozzoli@uniroma1.it

hand, for turbulent wall-bounded flows the application of the overlap framework requires a number of assumptions owing to the unclosed nature of the time-averaged equation(s). Given this proviso, however, the overlap layer approach is perhaps the most extensively employed to rationalize, for example, the existence of the logarithmic mean velocity profile, or in the case of passive scalar transport, the logarithmic mean scalar profile [3,4].

In contrast, direct examination of the mean momentum or mean scalar transport equations reveals the leading balance structure, and that this structure is associated with a layer arrangement distinct from that used in the overlap layer formulations [5–8]. The ensuing analyses that leverage this structure are mathematically characterized by considering the *actual* magnitude ordering of terms in the relevant mean equation as opposed to those formally implied by, for example, inner or outer normalization. Among the results found by employing this framework is that the second and third layers from the wall (for pipes and channels) have a width characterized by an intermediate length scale, i.e., $\sqrt{\nu\delta/u_\tau}$, and that in the last layer from the wall (layer IV) the molecular diffusion terms (mean viscous force or conductive heat flux) lose leading order significance. Here the mean momentum or mean scalar transport occurs predominantly by turbulent inertia or stirring. This domain is associated with a linearly varying hierarchy of scaling layers that underlies a self-similar structure formally admitted by the relevant mean equation (i.e., for scalar or momentum). Direct integration of this self-similar form of the mean equation leads to a logarithmic mean profile equation. Notably, this approach does not require invoking a closure hypothesis or other similar assumptions [8–11]. Consistently, a number statistical measures of self-similarity have been shown to coincide with the inertial portion of the layer hierarchy domain [12–15]. Here it is important to note that the existence of, and region where, *distance-from-the-wall* scaling holds is an analytical finding of this approach. This is significant since the assumption of distance-from-the-wall scaling is central to many turbulence modeling approaches, underlying, for example, Townsend's attached eddy hypothesis [16].

Following the general approach used for the mean momentum equation, Zhou *et al.* [17] explored the mean, turbulence, and total kinetic energy balance equations in the canonical turbulent channel, pipe, and boundary layer flows. The leading order balance structure of the mean kinetic energy equation was empirically characterized and mathematically verified to have a structure identical to that of the mean momentum equation. Zhou's analyses also showed that there exists a four-layer structure to the total kinetic energy budget equation, with the property that in each of these layers the leading balance occurs between a subset of the relevant grouped terms in that equation. This four-layer structure is, however, distinct from that of the mean momentum equation. For example, the third layer for the total kinetic energy balance is located in the inertial domain (as identified by the mean momentum equation) and has a layer thickness that grows at a rate proportional to $\delta - \sqrt{\nu\delta/u_\tau}$.

The present study extends the previous methodology to the total scalar variance equation for fully developed turbulent channel with uniform scalar generation. The ratio of the sum of the molecular transport term and the dissipation term to the gradient production/turbulent diffusion term is considered and reveals a four-layer structure for the total scalar variance equation. Both the Reynolds number- and Prandtl number-dependent properties of these layer thicknesses are then empirically quantified with DNS data, and some are analytically verified through a rescaling analysis. In the case where $\mathrm{Pr} = 1$, the mean scalar equation is identical to that for the mean momentum and has the same boundary conditions. The scalar Kármán constant, k_θ, is, however, empirically found to be greater than the Kármán constant, k, for the momentum field. A comparison between the streamwise velocity variance and scalar variance budget equations is investigated to show the different balance of terms across the corresponding inertial and nondiffusive domains. Owing to the analytical connection between the Kármán constant and the Reynolds stress (turbulent heat flux) elucidated by the present theoretical framework, the correlation coefficient profiles for both Reynolds shear stress and turbulent heat flux are also examined and interpreted on the self-similar inertial domain.

II. SCALAR VARIANCE EQUATION ANALYSIS

A. Basic equations

In the following, x denotes the streamwise direction, with the wall-normal direction given by y. Uppercase letters or angle brackets denote the averaged quantities, and lowercase letters indicate fluctuations about the mean. The x, y, and z velocity components are given by variants of u, v, and w, respectively, and δ is used to denote the half channel height.

In a Cartesian system, the time-averaged mean scalar variance and turbulence scalar variance equations are, respectively, given by

$$\frac{\partial}{\partial t}\left(\frac{1}{2}\Theta^2\right) + U_j\frac{\partial}{\partial x_j}\left(\frac{1}{2}\Theta^2\right) + \Theta\frac{\partial}{\partial x_j}\langle u_j\theta\rangle = \alpha\frac{\partial^2}{\partial x_j\partial x_j}\left(\frac{1}{2}\Theta^2\right) - \alpha\frac{\partial\Theta}{\partial x_j}\frac{\partial\Theta}{\partial x_j} + \Theta Q \tag{1}$$

and

$$\frac{\partial}{\partial t}\left(\frac{1}{2}\theta^2\right) + U_j\frac{\partial}{\partial x_j}\left(\frac{1}{2}\theta^2\right) + \langle u_j\theta\rangle\frac{\partial\Theta}{\partial x_j} + \frac{\partial}{\partial x_j}\left\langle u_j\frac{1}{2}\theta^2\right\rangle = \alpha\frac{\partial^2}{\partial x_j\partial x_j}\left\langle\frac{1}{2}\theta^2\right\rangle - \alpha\left\langle\frac{\partial\theta}{\partial x_j}\frac{\partial\theta}{\partial x_j}\right\rangle. \tag{2}$$

Here Θ is the mean scalar and θ is the fluctuating scalar (and similarly for the velocity components), α is the thermal diffusivity, and Q is the scalar generation per unit volume.

Statistically stationary and fully developed turbulent flow in a planar channel with uniform scalar generation is considered. Since this flow is both planar and fully developed, derivatives of averaged quantities with respect to x and z are zero, and mean quantities are solely a function of y. Under these conditions, the simplified form of the mean scalar variance equation for turbulent channel flow becomes

$$\alpha\frac{d^2}{dy^2}\left(\frac{1}{2}\Theta^2\right) - \Theta\frac{d}{dy}\langle v\theta\rangle - \alpha\frac{d\Theta}{dy}\frac{d\Theta}{dy} + \Theta Q = 0, \tag{3}$$

and similarly, the resulting simplified form of the turbulence scalar variance equation is given by

$$-\frac{d}{dy}\left\langle v\frac{1}{2}\theta^2\right\rangle + \alpha\frac{d^2}{dy^2}\left\langle\frac{1}{2}\theta^2\right\rangle - \langle v\theta\rangle\frac{d\Theta}{dy} - \alpha\left\langle\frac{\partial\theta}{\partial x_j}\frac{\partial\theta}{\partial x_j}\right\rangle = 0. \tag{4}$$

Inner normalization is applied to each term in Eqs. (3) and (4) with the friction scalar $\theta_\tau = \frac{\alpha}{u_\tau}\frac{d\Theta}{dy}|_{\text{wall}}$, friction velocity $u_\tau = \sqrt{\tau_{\text{wall}}/\rho}$, and ν,

$$\Theta^+ = \frac{\Theta}{\theta_\tau}, \quad \theta^+ = \frac{\theta}{\theta_\tau}, \quad v^+ = \frac{v}{u_\tau}, \quad -v^+\theta^+ = -\frac{v\theta}{u_\tau\theta_\tau}, \quad y^+ = \frac{yu_\tau}{\nu}, \quad \delta^+ = \frac{\delta u_\tau}{\nu}. \tag{5}$$

Under inner normalization Eq. (3) is

$$\underbrace{\frac{1}{\text{Pr}}\frac{d^2}{dy^{+2}}\left(\frac{1}{2}\Theta^{+2}\right)}_{\text{MMD}} \underbrace{+\Theta^+\frac{dT_\theta^+}{dy^+}}_{\text{PGT}} \underbrace{-\frac{1}{\text{Pr}}\frac{d\Theta^+}{dy^+}\frac{d\Theta^+}{dy^+}}_{\text{MD}} \underbrace{+\Theta^+\frac{1}{\delta^+}}_{\text{SG}} = 0, \tag{6}$$

where $T_\theta^+ = -\langle v^+\theta^+\rangle$. We identify these four terms, respectively, as mean molecular diffusion (MMD), production gradient of turbulent transport flux (PGT), mean dissipation (MD), and scalar generation (SG). Similarly, the inner-normalized Eq. (4) is

$$\underbrace{-\frac{d}{dy^+}\left\langle v^+\frac{1}{2}\theta^{+2}\right\rangle}_{\text{TD}} \underbrace{+\frac{1}{\text{Pr}}\frac{d^2}{dy^{+2}}\left\langle\frac{1}{2}\theta^{+2}\right\rangle}_{\text{TMT}} \underbrace{+T_\theta^+\frac{d\Theta^+}{dy^+}}_{\text{GP}} \underbrace{-\frac{1}{\text{Pr}}\left\langle\frac{\partial\theta^+}{\partial x_j^+}\frac{\partial\theta^+}{\partial x_j^+}\right\rangle}_{\text{TD}} = 0. \tag{7}$$

These four terms are, respectively, referred to as turbulent diffusion (TD), turbulent molecular transport (TMT), gradient production (GP), and turbulent dissipation (TD). Combination of Eqs. (6)

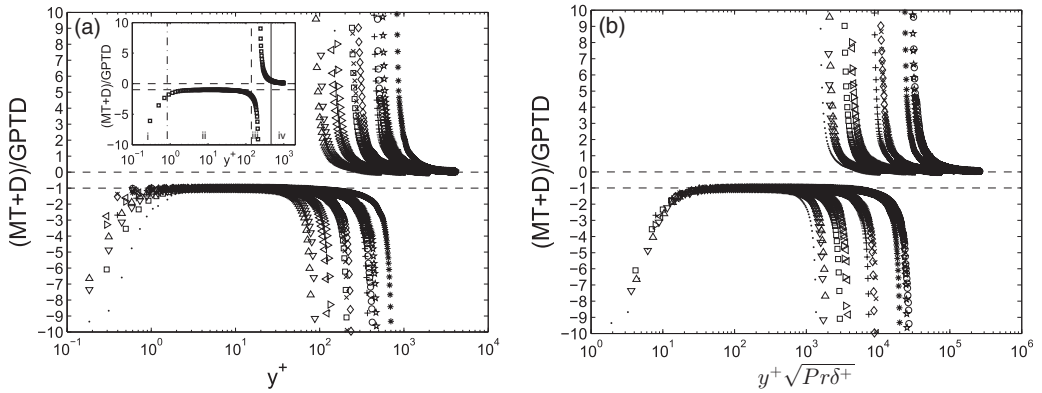

FIG. 1. (a) Ratio of the sum of the molecular transport (MT) and dissipation (D) terms to the gradient production/turbulent diffusion term (GPTD). Inset: Four-layer structure specifically presented by □, $\delta^+ = 995$, $\mathrm{Pr} = 0.20$, $\delta^+/\mathrm{Pr} = 4975$. Vertical dashed-dotted line denotes the external bound of layer i. Vertical dashed line denotes the external bound of layer ii. Vertical solid line denotes the external bound of layer iii. (b) Ratio of the sum of the molecular transport (MT) and dissipation (D) terms to the gradient production/turbulent diffusion term (GPTD) versus $y^+\sqrt{\mathrm{Pr}\delta^+}$. DNS data are from Pirozzoli *et al.* [18]: △, $\delta^+ = 548$, $\mathrm{Pr} = 1$, $\delta^+/\mathrm{Pr} = 548$; ▽, $\delta^+ = 548$, $\mathrm{Pr} = 0.71$, $\delta^+/\mathrm{Pr} = 772$; ◁, $\delta^+ = 995$, $\mathrm{Pr} = 1$, $\delta^+/\mathrm{Pr} = 995$; ▷, $\delta^+ = 995$, $\mathrm{Pr} = 0.71$, $\delta^+/\mathrm{Pr} = 1401$; ×, $\delta^+ = 2017$, $\mathrm{Pr} = 1$, $\delta^+/\mathrm{Pr} = 2017$; ·, $\delta^+ = 548$, $\mathrm{Pr} = 0.20$, $\delta^+/\mathrm{Pr} = 2740$; ◇, $\delta^+ = 2017$, $\mathrm{Pr} = 0.71$, $\delta^+/\mathrm{Pr} = 2841$; ○, $\delta^+ = 4088$, $\mathrm{Pr} = 1$, $\delta^+/\mathrm{Pr} = 4088$; □, $\delta^+ = 995$, $\mathrm{Pr} = 0.20$, $\delta^+/\mathrm{Pr} = 4975$; ☆, $\delta^+ = 4088$, $\mathrm{Pr} = 0.71$, $\delta^+/\mathrm{Pr} = 5758$; +, $\delta^+ = 2017$, $\mathrm{Pr} = 0.20$, $\delta^+/\mathrm{Pr} = 10085$; ✳, $\delta^+ = 4088$, $\mathrm{Pr} = 0.20$, $\delta^+/\mathrm{Pr} = 20\,440$.

and (7) gives the inner-normalized total scalar variance equation

$$\underbrace{\frac{1}{\mathrm{Pr}}\frac{d^2}{dy^{+2}}\left[\frac{1}{2}\Theta^{+2}+\left\langle\frac{1}{2}\theta^{+2}\right\rangle\right]}_{\mathrm{MT}}+\underbrace{\frac{d}{dy^+}\left[\Theta^+T_\theta^+-\left\langle v^+\frac{1}{2}\theta^{+2}\right\rangle\right]}_{\mathrm{GPTD}}$$
$$+\underbrace{\left[-\frac{1}{\mathrm{Pr}}\frac{d\Theta^+}{dy^+}\frac{d\Theta^+}{dy^+}-\frac{1}{\mathrm{Pr}}\left\langle\frac{\partial\theta^+}{\partial x_j^+}\frac{\partial\theta^+}{\partial x_j^+}\right\rangle\right]}_{D}\underbrace{+\Theta^+\frac{1}{\delta^+}}_{\mathrm{PG}}=0. \tag{8}$$

The four grouped terms are respectively referred to as molecular transport (MT), gradient production/turbulent diffusion (GPTD), dissipation (D), and product scalar generation (PG).

B. Four-layer structure

As guided by our previous study of the total kinetic energy budget equation [17], the ratio of the sum of the molecular transport term and the dissipation term to the gradient production/turbulent diffusion term (MT+D)/GPTD is used to characterize the layer structure of the total scalar variance equation. As can be seen, the data organize into four clear layers, which we label layers i–iv. Consistent with the criterion used in the previous analysis, the ending position of layer i is where this ratio becomes greater than -2. The external bound of layer ii is determined where the ratio is less than -2, while the outer boundary of layer iii is based on where the ratio decreases below 0.5. The ratio profiles are shown in Fig. 1(a). Layer i lies close to the wall, $y^+ \lesssim 1$. In this domain, the leading balance is between the molecular transport term and the dissipation term. Consistent with the first layer associated with the mean scalar equation structure, the thermal inner length scale, $\sqrt{\nu^2\alpha/u_\tau^3\delta}$, also scales the first layer (layer i) of Eq. (8). The scaling with this length is

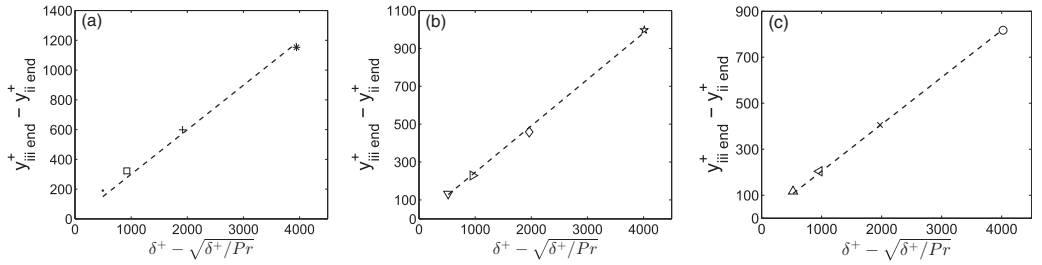

FIG. 2. (a) Inner-normalized width of layer iii for $\mathrm{Pr} = 0.20$. $\cdot$, $\delta^+ = 548$, $\mathrm{Pr} = 0.20$, $\delta^+/\mathrm{Pr} = 2740$; $\square$, $\delta^+ = 995$, $\mathrm{Pr} = 0.20$, $\delta^+/\mathrm{Pr} = 4975$; $+$, $\delta^+ = 2017$, $\mathrm{Pr} = 0.20$, $\delta^+/\mathrm{Pr} = 10\,085$; $\ast$, $\delta^+ = 4088$, $\mathrm{Pr} = 0.20$, $\delta^+/\mathrm{Pr} = 20\,440$. Curve fit is given by $0.29(\delta^+ - \sqrt{\delta^+/\mathrm{Pr}})$. (b) Inner-normalized width of layer iii for $\mathrm{Pr} = 0.71$. $\bigtriangledown$, $\delta^+ = 548$, $\mathrm{Pr} = 0.71$, $\delta^+/\mathrm{Pr} = 772$; $\triangleright$, $\delta^+ = 995$, $\mathrm{Pr} = 0.71$, $\delta^+/\mathrm{Pr} = 1401$; $\diamond$, $\delta^+ = 2017$, $\mathrm{Pr} = 0.71$, $\delta^+/\mathrm{Pr} = 2841$; $\star$, $\delta^+ = 4088$, $\mathrm{Pr} = 0.71$, $\delta^+/\mathrm{Pr} = 5758$. Curve fit is given by $0.25(\delta^+ - \sqrt{\delta^+/\mathrm{Pr}})$. (c) Inner-normalized width of layer iii for $\mathrm{Pr} = 1$. $\bigtriangleup$, $\delta^+ = 548$, $\mathrm{Pr} = 1$, $\delta^+/\mathrm{Pr} = 548$; $\triangleleft$, $\delta^+ = 995$, $\mathrm{Pr} = 1$, $\delta^+/\mathrm{Pr} = 995$; $\times$, $\delta^+ = 2017$, $\mathrm{Pr} = 1$, $\delta^+/\mathrm{Pr} = 2017$; $\circ$, $\delta^+ = 4088$, $\mathrm{Pr} = 1$, $\delta^+/\mathrm{Pr} = 4088$. Curve fit is given by $0.21(\delta^+ - \sqrt{\delta^+/\mathrm{Pr}})$.

convincingly reflected in Fig. 1(b). A curve fit indicates that $y^+_{i\mathrm{end}}$ varies like $12.58\,\mathrm{Pe}_\tau^{-\frac{1}{2}}$, where $\mathrm{Pe}_\tau = \mathrm{Pr}\delta^+$ is the friction Péclet number. Outside layer i, the ratio of Fig. 1 is very close to -1, and even more so at the highest δ^+. Across this region (layer ii), the molecular transport, dissipation, and the gradient production/turbulent diffusion terms constitute the leading balance. Commensurate with the gradient production/turbulent diffusion term changing its sign, there is a leading balance exchange across layer iii. Detailed examination (not shown) indicates that, except for the molecular diffusion term, the other three terms are leading order. With greater distance from the wall, the magnitude of the dissipation term becomes much smaller, and its loss of leading order marks the onset of layer iv. This last layer is where the gradient production/turbulent diffusion term is balanced by the scalar generation term.

C. Width of layer iii

As demonstrated in Fig. 1, layer iii is where the leading balance transitions from one in which molecular effects are important to one where these effects become subdominant. As such this layer width is expected to exhibit sensitivity to both Reynolds and Prandtl number. The Reynolds and Prandtl number dependencies of the inner-normalized width of layer iii are shown in Figs. 2(a)–2(c) for $\mathrm{Pr} = 0.20$, 0.71, and 1, respectively. Consistent with the scaling analysis in Sec. II E below, here the inner-normalized width of layer iii is plotted for fixed Pr and versus $\delta^+ - \sqrt{\delta^+/\mathrm{Pr}}$. This is reasoned to effectively account for the finite Reynolds number effect on the outer normalization. For fixed Pr, the inner-normalized width of layer iii increases according to a linear trend in $\delta^+ - \sqrt{\delta^+/\mathrm{Pr}}$. We note, however, that the leading coefficients in these linear relations are different for each Pr.

D. Balances in layers iii and iv

Close examination indicates that across layers iii and iv, the contribution to Eq. (8) from turbulent diffusion is much smaller than the contribution from gradient production. This observation is exemplified by the $\delta^+ = 4088$, $\mathrm{Pr} = 0.2$ results of Fig. 3(a). It is surmised that in layers iii and iv the turbulent diffusion term is subdominant and the dissipation term is dominated by its turbulence contribution. This is demonstrated in Fig. 3(b), which shows the ratio of the mean to turbulent dissipation (MD/TD). In these figures, the data curves consistently segregate into three Prandtl number-dependent groups. The vertical dashed-dotted, dashed, and solid lines, respectively,

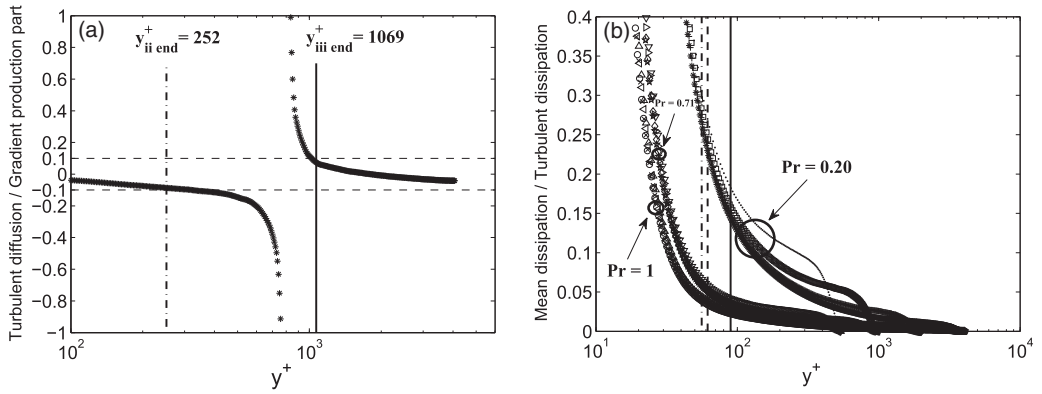

FIG. 3. (a) Ratio of the turbulent diffusion to the gradient production part at $\delta^+ = 4088$, Pr $= 0.20$, $\delta^+/\mathrm{Pr} = 20440$. The vertical dashed-dotted line denotes the external bound of layer ii. The vertical solid line denotes the external bound of layer iii. (b) Ratio of the mean dissipation (MD) to the turbulent dissipation (TD). The vertical dashed-dotted line denotes the external bound of layer ii at $\delta^+ = 548$, Pr $= 1$, $\delta^+/\mathrm{Pr} = 548$. The vertical dashed line denotes the external bound of layer ii at $\delta^+ = 548$, Pr $= 0.71$, $\delta^+/\mathrm{Pr} = 772$. The vertical solid line denotes the external bound of layer ii at $\delta^+ = 548$, Pr $= 0.20$, $\delta^+/\mathrm{Pr} = 2740$.

represent the end of layer ii for $\delta^+ = 548$, Pr $= 1$ ($\delta^+/\mathrm{Pr} = 548$), $\delta^+ = 548$, Pr $= 0.71$ ($\delta^+/\mathrm{Pr} = 772$) and $\delta^+ = 548$, Pr $= 0.20$ ($\delta^+/\mathrm{Pr} = 2740$). Beyond the start of layer iii the mean dissipation is at least six times smaller than the turbulent dissipation, and its effect over layer iii diminishes with increasing δ^+. As a result, the layer iii balance simplifies to being composed of PGT, GP, TD, and SG. Figure 4(a) shows profiles of these four terms across layers iii and iv at $\delta^+ = 4088$. Beyond layer iii, GP and TD lose leading order, becoming negligible compared to PGT and SG. Figure 4(b) shows the profile of PGT/SG and the ratio of GP/TD.

As might be expected from the classical production equals turbulence dissipation argument, although both the GP and TD terms are much smaller than the other two terms (and thus are not leading order), their ratio is nearly -1. This ratio then approaches zero near the outer edge of layer iv. Beyond layer ii, the GP term, is balanced by the TD term with the gradient production term

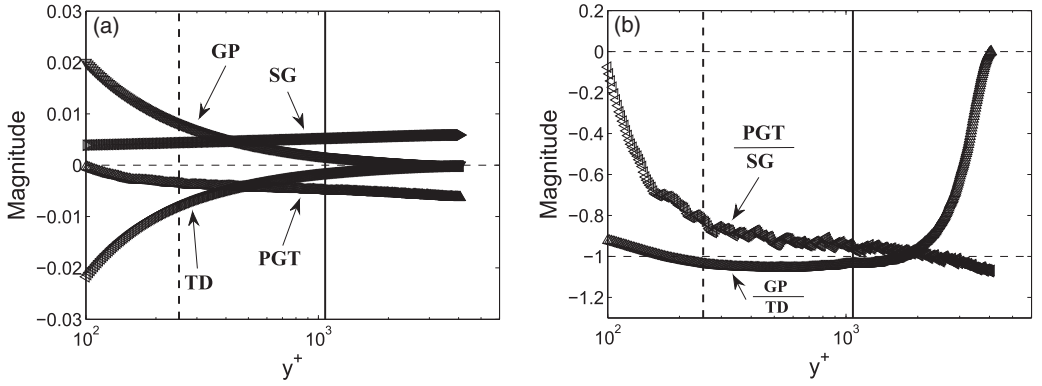

FIG. 4. (a) Profiles of terms PGT ($\bigtriangleup$), GP ($\bigtriangledown$), TD ($\triangleleft$), and SG ($\triangleright$) across layers iii and iv at $\delta^+ = 4088$, Pr $= 1$, $\delta^+/\mathrm{Pr} = 4088$. The vertical dashed-dotted line denotes the external bound of layer ii. The vertical solid line denotes the external bound of layer iii. (b) Ratios of terms PGT/SG ($\triangleleft$) and GP/TD at $\delta^+ = 4088$, Pr $= 1$, $\delta^+/\mathrm{Pr} = 4088$. The vertical dashed-dotted line denotes the external bound of layer ii. The vertical solid line denotes the external bound of layer iii.

approaching 0 more rapidly as $y^+ \to \delta^+$. The ratio of the PGT to the SG term is also approximately -1 throughout layer iv. It is concluded that beyond layer ii, the PGT term nominally balances the SG term. The two separate combinations of terms just described respectively reflect the approximate balances associated with the mean and turbulence scalar variance equations. Here we note that while the predominant focus of research has been on the turbulence equations, it is in fact the mean terms that dominate on layer iv.

E. Analytical estimate of the characteristic length of layer iii

This section presents an analysis revealing that $(\delta^+ - \sqrt{\delta^+/\mathrm{Pr}})$ is the appropriate length for scaling the width of layer iii. We firstly note that layer iii is located in the nondiffusive domain associated with the similarity solution of the mean scalar transport equation. Zhou *et al.* [8] showed that on this domain the mean scalar equation can be written in an invariant form that without further simplifications or assumptions can be twice integrated. Over this domain, these integrations yield the logarithmic mean scalar profile equation

$$\Theta^+ = \phi_{\theta c}^2 \, \ln(y^+ - C_1) + C_2 y^+ + C_3. \tag{9}$$

For $\delta^+ \to \infty$, Zhou *et al.* [8] demonstrate that Eq. (9) reduces to the classical approximation, $\Theta^+ = \frac{1}{k_\theta} \ln y^+ + C_3$, where $k_\theta = \phi_{\theta c}^{-2}$. For the present purpose, we now work backwards to obtain a relation for dT_θ^+/dy^+. Two differentiations yield

$$\frac{1}{\mathrm{Pr}} \frac{d^2\Theta^+}{dy^{+2}} = -\frac{1}{\mathrm{Pr}} \frac{\phi_{\theta c}^2}{(y^+ - C_1)^2}. \tag{10}$$

Inserting this relation into the mean scalar equation [8] allows one to write

$$\frac{dT_\theta^+}{dy^+} = -\frac{1}{\mathrm{Pr}} \frac{d^2\Theta^+}{dy^{+2}} - \epsilon^2 = \frac{1}{\mathrm{Pr}} \frac{\phi_{\theta c}^2}{(y^+ - C_1)^2} - \epsilon^2, \tag{11}$$

where $\epsilon^2 = 1/\delta^+$. We now employ the condition that T_θ^+ attains its maximum at $y_{\theta m}^+$, i.e., in the center part of the third layer associated with the mean scalar equation. Here $dT_\theta^+/dy^+ = 0$. This condition leads to $\epsilon^2 = \frac{1}{\mathrm{Pr}} \frac{\phi_{\theta c}^2}{(y_{\theta m}^+ - C_1)^2}$, and Eq. (11) becomes

$$\frac{dT_\theta^+}{dy^+} = \frac{1}{\mathrm{Pr}} \frac{\phi_{\theta c}^2}{(y^+ - C_1)^2} - \frac{1}{\mathrm{Pr}} \frac{\phi_{\theta c}^2}{(y_{\theta m}^+ - C_1)^2}. \tag{12}$$

Integration of Eq. (12) leads to

$$T_\theta^+ = C_4 - \frac{1}{\mathrm{Pr}} \frac{\phi_{\theta c}^2}{y^+ - C_1} - \frac{1}{\mathrm{Pr}} \frac{\phi_{\theta c}^2 y^+}{(y_{\theta m}^+ - C_1)^2}. \tag{13}$$

Noting that C_1 becomes negligible as $\delta^+ \to \infty$ and using $y_{\theta m}^+ = H\sqrt{\delta^+/\mathrm{Pr}}$ [where H is an $O(1)$ constant, $\simeq$1.48 [8]] give

$$\frac{dT_\theta^+}{dy^+} = \frac{1}{\mathrm{Pr}} \frac{\phi_{\theta c}^2}{y^{+2}} - \frac{\phi_{\theta c}^2}{H^2 \delta^+} \tag{14}$$

and thus

$$T_\theta^+ = C_4 - \frac{1}{\mathrm{Pr}} \frac{\phi_{\theta c}^2}{y^+} - \frac{\phi_{\theta c}^2 y^+}{H^2 \delta^+}. \tag{15}$$

Using $T_\theta^+ = 0$ at $y^+ = \delta^+$ as $\delta^+ \to \infty$ for any fixed Pr allows evaluation of C_4,

$$C_4 = \frac{\phi_{\theta c}^2}{H^2}. \tag{16}$$

Similarly, using $T_\theta^+ = 1$ at $y^+ = y_{\theta m}^+ = H\sqrt{\delta^+/\mathrm{Pr}}$ as $\delta^+ \to \infty$ for any Pr yields

$$1 = \frac{\phi_{\theta c}^2}{H^2}, \tag{17}$$

and thus $C_4 \to 1$ as $\delta^+ \to \infty$.

We now use these findings to characterize the scaling of the leading balance of Eq. (8) in layer iii. Noting that $\Theta^+(dT_\theta^+/dy^+) \sim \epsilon^2\Theta^+$ in layer iii gives

$$\frac{dT_\theta^+}{dy^+} = \frac{1}{\mathrm{Pr}}\frac{\phi_{\theta c}^2}{y^{+2}} - \frac{\phi_{\theta c}^2}{H^2\delta^+} = O(\epsilon^2). \tag{18}$$

As $\delta^+ \to \infty$, $\phi_{\theta c}^2$ and $\phi_{\theta c}^2/H^2$ both remain $O(1)$, Eq. (26) is valid only when $y^+ \geqslant O(1/\sqrt{\mathrm{Pr}}\epsilon) = O(\sqrt{\delta^+/\mathrm{Pr}})$. Thus, requiring $y^+ \geqslant O(1/\sqrt{\mathrm{Pr}}\epsilon)$ in Eq. (13) and noting that C_4 is $O(1)$ gives

$$T_\theta^+ = O\left(1 - \frac{\epsilon}{\sqrt{\mathrm{Pr}}}\right) \tag{19}$$

in layer iii. This order of magnitude is valid in the portion of layer iii that is beyond the peak of T_θ^+, since $T_{\theta m}^+$ is $1 - O(\epsilon/\sqrt{\mathrm{Pr}})$.

Within layer iii, Eq. (18) shows that

$$\frac{dT_\theta^+}{dy^+} = O(\epsilon^2). \tag{20}$$

Thus, our task now is to find a rescaling that formally reflects both terms as leading order. The rescaling process begins by setting

$$T^+ = R\bar{T}, \quad y^+ = y_0^+ + S\bar{y}, \tag{21}$$

where $\bar{T}$, $\bar{y}$ are $O(1)$ as $\delta^+ \to \infty$, and y_0^+ is the position where the gradient production/turbulent diffusion term changes its sign in layer iii. Inserting Eqs. (21) into Eq. (20) gives

$$\frac{dT_\theta^+}{dy^+} = \frac{R}{S}\frac{d\bar{T}}{d\bar{y}}. \tag{22}$$

As a result, rendering this expression $O(1)$ requires that

$$S = \frac{1}{\epsilon^2}R. \tag{23}$$

Note that R is the order of T_θ^+ in layer iii, that is $1 - \epsilon/\sqrt{\mathrm{Pr}}$, and thus S is then found to be

$$S = \frac{1}{\epsilon^2}\left(1 - \frac{\epsilon}{\sqrt{\mathrm{Pr}}}\right). \tag{24}$$

Using this in the y-scaling of Eq. (21) gives

$$y^+ = y_0^+ + \left(\frac{1}{\epsilon^2} - \frac{1}{\epsilon\sqrt{\mathrm{Pr}}}\right)\bar{y} = y_0^+ + \left(\delta^+ - \sqrt{\frac{\delta^+}{\mathrm{Pr}}}\right)\bar{y}. \tag{25}$$

By definition, $\bar{y}$ is $O(1)$ in layer iii, and thus it follows that the inner-normalized width of layer iii is $O(\delta^+ - \sqrt{\delta^+/\mathrm{Pr}})$ for any fixed Pr. This scaling is interpreted as a finite Reynolds number correction to traditional outer scaling, since it is apparent that $(\delta^+ - \sqrt{\delta^+/\mathrm{Pr}}) \to \delta^+$ for fixed Pr as $\delta^+ \to \infty$.

III. ON THE DIFFERENCE BETWEEN THE SCALAR AND MOMENTUM KÁRMÁN CONSTANTS

The findings herein, along with our previous studies of the mean scalar equation, allow us to extract results pertaining to the known difference between the logarithmic mean scalar and velocity profiles. The present simulations provide a unique opportunity to examine this issue, as these simulations are, to the authors' knowledge, the first to show that even when the mean scalar and velocity problems constitute an identical boundary value problem, a distinct difference between k and k_θ remains. The identical scalar and velocity boundary value problem leads one to naively expect that the scalar Kármán constant should be numerically the same as that for the momentum field. Notably, however, both the direct slope measurements by Pirozzoli *et al.* [18] and the mean equation analysis by Zhou *et al.* [8] indicate that the scalar Kármán constant for $\mathrm{Pr} = 1$ is $k_\theta > 0.45$, while for the velocity $k \simeq 0.39$. For well-posed determinate systems, an identical equation with identical boundary conditions will yield an identical solution. Here, of course, the indeterminacy of the mean equations is operative.

The analytical framework employed herein provides a refined basis for elucidating the noted difference between k and k_θ. This approach explicitly describes how the value of the profile slope constant for the velocity or scalar is connected to the profile of the Reynolds stress or scalar flux, respectively. Specifically, analytical treatment of the mean equations reveals that the discrepancy between k_θ ($\mathrm{Pr} = 1$) and k derives from small differences between the wall-normal gradients of these functions on the inertial (nondiffusive) domain.

The decay rate of these functions determine the characteristic length distributions that respectively underly the logarithmic dependence of the mean profiles [19]. For each case, the distribution of lengths describes the widths of a hierarchy of scaling layers. For the velocity and scalar these are, respectively, denoted W^+ and W_θ^+ [see Eqs. (26) and (27)]. Both are functions of y^+. The layer width distributions analytically derive from determining an invariant form of the mean equation that holds on each layer of the hierarchy. While this invariant form is valid across a domain that extends from near the edge of the viscous sublayer to beyond the logarithmic layer, our present focus is on the inertial (nondiffusive) domain. Here the analysis reveals that $W^+(y^+)$ or $W_\theta^+(y^+)$ asymptotically attain proportionality with the distance from the wall, and at any finite δ^+ they best approximate linearity on this domain. To the authors' knowledge, these analyses yield the only analytical basis for *distance from the wall scaling*. The invariance of the mean equation and this associated property underlies a similarity solution found by directly integrating the mean equations (for velocity or scalar) on the inertial domain. Relevant to the present aims, these analyses also reveal that the values of k and k_θ are directly related to dW^+/dy^+ and dW_θ^+/dy^+, respectively. Namely, $k = (dW^+/dy^+)^2$ on the inertial domain, and similarly $k_\theta = (dW_\theta^+/dy^+)^2$.

The respective relationships between W^+ and W_θ^+ and the Reynolds stress and scalar flux gradients are seen through their definitions [8,9]

$$W^+ = \left(\frac{dT^+}{dy^+} + \frac{1}{\delta^+}\right)^{-\frac{1}{2}} \tag{26}$$

and

$$W_\theta^+ = \left(\frac{dT_\theta^+}{dy^+} + \frac{1}{\delta^+}\right)^{-\frac{1}{2}}, \tag{27}$$

where $T^+ = -\langle u^+ v^+ \rangle$ and $T_\theta^+ = -\langle v^+ \theta^+ \rangle$. The only difference in these expressions comes from those between dT^+/dy^+ and dT_θ^+/dy^+. Since the v fluctuations are unchanged in a flow with a passive scalar, the differences in the transport of the u and the θ fluctuations, and/or their correlation with the v fluctuations, account for the difference between the gradients of Reynolds stress and turbulent scalar flux on the nondiffusive domain of interest. In what follows, we first expose the primary reason why the Reynolds stress and scalar flux gradients are different on the inertial domain,

and then investigate the differences between the u and θ fluctuation statistics and their associated effect on the Reynolds stress and scalar flux.

A. Composition of the Reynolds stress and scalar flux gradients

Product rule expansion of the Reynolds stress and scalar flux gradients yields

$$\frac{dT^+}{dy^+} = -\left\langle v^+ \frac{\partial u^+}{\partial y^+} \right\rangle - \left\langle u^+ \frac{\partial v^+}{\partial y^+} \right\rangle \tag{28}$$

and

$$\frac{dT_\theta^+}{dy^+} = -\left\langle v^+ \frac{\partial \theta^+}{\partial y^+} \right\rangle - \left\langle \theta^+ \frac{\partial v^+}{\partial y^+} \right\rangle, \tag{29}$$

respectively. These representations are useful since they identify the second term with the continuity constraint on the velocity field. As discussed further below, this factors into how u and v correlate in a manner different from θ and v. Regarding Eq. (28) it is also relevant to note that for fully developed channel flow

$$\frac{dT^+}{dy^+} = \langle v^+ \omega_z^+ \rangle - \langle w^+ \omega_y^+ \rangle, \tag{30}$$

where ω_z^+ and ω_y^+ are the spanwise and wall-normal vorticity fluctuations, respectively. Recalling the definitions of these vorticity components reveals that the terms on the right-hand side of Eqs. (28) and (30) are identically equal to each other. This is obvious for the first terms, but one must invoke continuity to show that the second terms are equal to each other. The representation of the Reynolds stress gradient in Eq. (30) is physically significant. Here the first term is associated with the turbulent wall-normal advection of spanwise vorticity, while the second term embodies change of scale effects associated with vorticity stretching and reorientation [3,20].

With this as context, we now compare the analogous terms on the right-hand side of Eqs. (28) and (29). Figure 5(a) displays these profiles at $\delta^+ = 4088$ over the entire half-channel, and Fig. 5(b) shows a close-up of these profiles on the inertial domain. In combination, Figs. 5(a) and 5(b) show that the profiles of $\langle v^+ \partial u^+/\partial y^+ \rangle$ and $\langle v^+ \partial \theta^+/\partial y^+ \rangle$ are nearly identical, while on the inertial domain $\langle u^+ \partial v^+/\partial y^+ \rangle$ is distinctly different from $\langle \theta^+ \partial v^+/\partial y^+ \rangle$. Physically, these findings indicate that the wall-normal turbulent advection of scalar and spanwise vorticity are on average very similar, while the average change of scale effects on the inertial domain are significantly different. According to Eqs. (26) and (27), this discrepancy accounts for the observed difference between k and k_θ.

B. Streamwise velocity variance budget versus scalar variance budget

The differences between the streamwise velocity and scalar fluctuations have been studied by a number of researchers [18,21,22]. Relative to the present aims, it is useful to examine the respective budget equations for $\langle u^2 \rangle$ and $\langle \theta^2 \rangle$.

The inner-normalized streamwise velocity variance budget equation for fully developed turbulent channel flow is

$$-\frac{d}{dy^+}\langle u^+ u^+ v^+ \rangle + \frac{d^2}{dy^{+2}}\langle u^+ u^+ \rangle + 2T^+ \frac{dU^+}{dy^+} - 2\left\langle \frac{\partial u^+}{\partial x_k^+} \frac{\partial u^+}{\partial x_k^+} \right\rangle + 2\left\langle p^+ \frac{\partial u^+}{\partial x^+} \right\rangle = 0. \tag{31}$$

As expected, this equation has five terms of a form similar to those found in the turbulence kinetic energy equation. The five terms are referred to as turbulent diffusion, viscous diffusion, production, dissipation, and pressure strain.

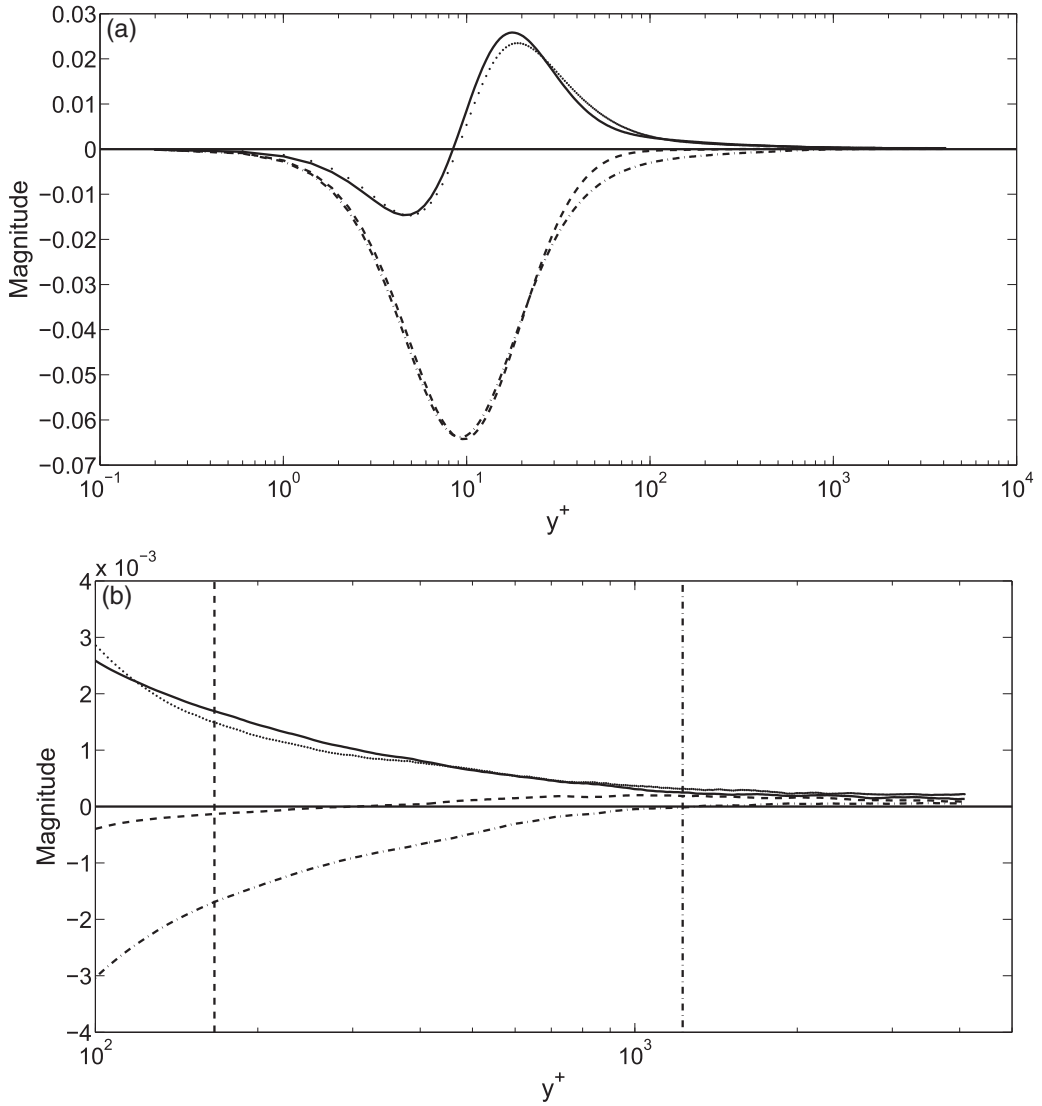

FIG. 5. (a) Profiles of terms on the right of Eq. (28) at $\delta^+ = 4088$. Profiles of terms on the right-hand side of Eq. (29) at $\delta^+ = 4088$ and $\mathrm{Pr} = 1$. Solid line, $\langle v^+ \partial u^+/\partial y^+ \rangle$; dotted line, $\langle v^+ \partial \theta^+/\partial y^+ \rangle$; dashed line, $\langle u^+ \partial v^+/\partial y^+ \rangle$; dashed-dotted line, $\langle \theta^+ \partial v^+/\partial y^+ \rangle$. (b) Closeup plot of (a) across inertial (nondiffusive) domain. The vertical dashed line denotes $y^+ = 2.6\sqrt{\delta^+}$. The vertical dashed-dotted line denotes $y^+ = 0.3\delta^+$.

The analogous inner-normalized scalar variance budget equation with uniform scalar generation which is two times Eq. (7) is

$$-\frac{d}{dy^+}\langle v^+\theta^+\theta^+\rangle + \frac{1}{\mathrm{Pr}}\frac{d^2}{dy^{+2}}\langle \theta^+\theta^+\rangle + 2T_\theta^+\frac{d\Theta^+}{dy^+} - 2\frac{1}{\mathrm{Pr}}\left\langle \frac{\partial\theta^+}{\partial x_k^+}\frac{\partial\theta^+}{\partial x_k^+}\right\rangle = 0. \tag{32}$$

The four terms are referred to as turbulent diffusion, molecular transport, gradient production, and dissipation.

There are five terms in the $\langle u^2\rangle^+$ budget equation, while there are only four terms in the $\langle \theta^2\rangle^+$ budget equation. As is apparent, the pressure-strain terms play a nontrivial role in streamwise

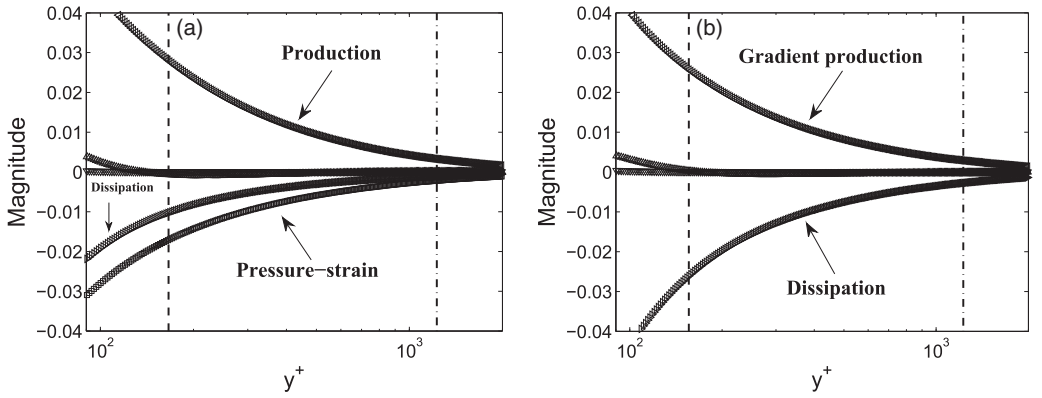

FIG. 6. (a) Profiles of terms in Eq. (31) across inertial domain at $\delta^+ = 4088$. $\bigtriangleup$, turbulent diffusion; $\bigtriangledown$, viscous diffusion; $\triangleleft$, production; $\triangleright$, dissipation; $\square$, pressure strain. The vertical dashed line denotes the external bound of layer III for mean momentum balance. The vertical dashed-dotted line denotes $y^+ = 0.3\delta^+$. (b) Profiles of terms in Eq. (32) across nondiffusive domain at $\delta^+ = 4088$ and $\mathrm{Pr} = 1$. $\bigtriangleup$, turbulent diffusion; $\bigtriangledown$, molecular transport; $\triangleleft$, gradient production; $\triangleright$, dissipation. The vertical dashed line denotes the external bound of layer III for mean scalar balance. The vertical dashed-dotted line denotes $y^+ = 0.3\delta^+$.

velocity transport. Since the similarity solution for both the mean velocity and mean scalar are valid over the inertial domain, the leading balance for the budget equations, Eqs. (28) and (29), are considered in this region. Specifically, this region is demarcated by $2.6\sqrt{\delta^+} \lesssim y^+ \lesssim 0.3\delta^+$ for the velocity, and $2.5\sqrt{\delta^+/\mathrm{Pr}} \lesssim y^+ \lesssim 0.3\delta^+$ (with $\mathrm{Pr} = 1$), for the scalar [8,19]. Figures 6(a) and 6(b), respectively, show representative profiles of the terms in Eqs. (31) and (32) across the noted domains. Similar production and generation production profiles are observed across this domain. The $\langle uu \rangle^+$ budget in the logarithmic region of the mean velocity profile is characterized by the leading balance of three terms, production, dissipation, and pressure strain. However, only the dissipation term balances the gradient production terms in the logarithmic region of the mean scalar profile. The magnitude of the streamwise velocity dissipation is considerably less than that of the scalar dissipation. This difference is physically compensated by the pressure strain. The findings of the previous subsection suggest that this is related to the differences in the change of scale effects on the vorticity versus scalar fields. The negative work done by the fluctuating pressure of the turbulence and the lower streamwise velocity dissipation rate play a role in generating a higher mean gradient for the velocity relative to the mean scalar gradient, i.e., $k < k_\theta$. This is consistent with the observation of Pirozzoli *et al.* [18], showing that the instantaneous cross-stream visualizations of θ exhibit much sharper internal interfaces than exhibited by the u field. This observation is also presumably related to the lower dissipation and the work done by the pressure on the inertial domain.

C. Correlation

Streamwise velocity variance profiles and scalar variance profiles for $\mathrm{Pr} = 1$ are shown in Fig. 7(a). The $\langle u^2 \rangle^+$ profiles attain distinctly larger values than the $\langle \theta^2 \rangle^+$ profiles on the internal domain, and tend towards a plateau just prior to the approximately logarithmic decay. The Reynolds stress, T^+, and turbulent flux, T_θ^+ profiles of Fig. 7(b), are, however, nearly indistinguishable from each other. A subtle difference between T^+ and T_θ^+ is observed in the inertial domain (see inset), where the T_θ^+ is larger. It is this subtle difference that modifies the hierarchy length scale distribution described by Eq. (26) versus Eq. (27), and as reflected in the differences in the contributions to dT^+/dy^+ and dT_θ^+/dy^+ in Fig. 5.

Given the relatively large differences between the $\langle u^2 \rangle^+$ and $\langle \theta^2 \rangle^+$ profiles, it is remarkable that the net inner-normalized correlation between u and v and θ and v is nearly identical. To understand

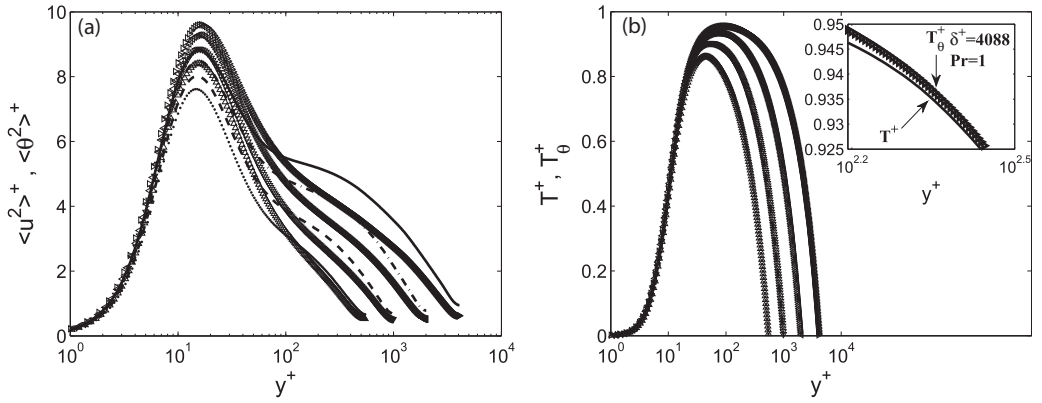

FIG. 7. (a) Streamwise velocity and scalar variances. Dotted line, $\langle u^2\rangle^+$, $\delta^+ = 548$; Dashed line, $\langle u^2\rangle^+$, $\delta^+ = 995$; dashed-dotted line, $\langle u^2\rangle^+$, $\delta^+ = 2017$; solid line, $\langle u^2\rangle^+$, $\delta^+ = 4088$; $\bigtriangleup$, $\langle\theta^2\rangle^+$, $\delta^+ = 548$, Pr $= 1$; $\bigtriangledown$, $\langle\theta^2\rangle^+$, $\delta^+ = 995$, Pr $= 1$; $\triangleleft$, $\langle\theta^2\rangle^+$, $\delta^+ = 2017$, Pr $= 1$; $\triangleright$, $\langle\theta^2\rangle^+$, $\delta^+ = 4088$, Pr $= 1$. (b) Reynolds stress and turbulent flux. Inset: Solid line, T^+, $\delta^+ = 4088$; $\triangleright$, T^+_θ, $\delta^+ = 4088$, Pr $= 1$.

this further we consider the associated correlation coefficient. This statistic is defined by

$$C_{ab} = \frac{\langle ab\rangle}{\sqrt{\langle a^2\rangle}\sqrt{\langle b^2\rangle}}. \tag{33}$$

It is the ratio of the covariance to the product of the respective standard deviations. The profiles of $-C_{uv}$ and $-C_{v\theta}$ for varying δ^+ and Pr $= 1$ are shown in Fig. 8(a) and specifically for $\delta^+ =$ 4088 in Fig. 8(b). In the logarithmic region, both $-C_{uv}$ and $-C_{v\theta}$ stay relatively close to 0.4, but increase with distance from the wall, and consistent with previous observations display a reduction in magnitude with increasing δ^+ [23]. The upward increment of $-C_{v\theta}$ on the inertial domain is, however, significantly greater than that of $-C_{uv}$. Here θ becomes more linearly correlated with v than does u. The noted difference is, however, much greater than that observed in Fig. 6(b), and this increased "efficiency" of the correlation nearly compensates for the amplitude differences shown in the profiles of Fig. 6(a).

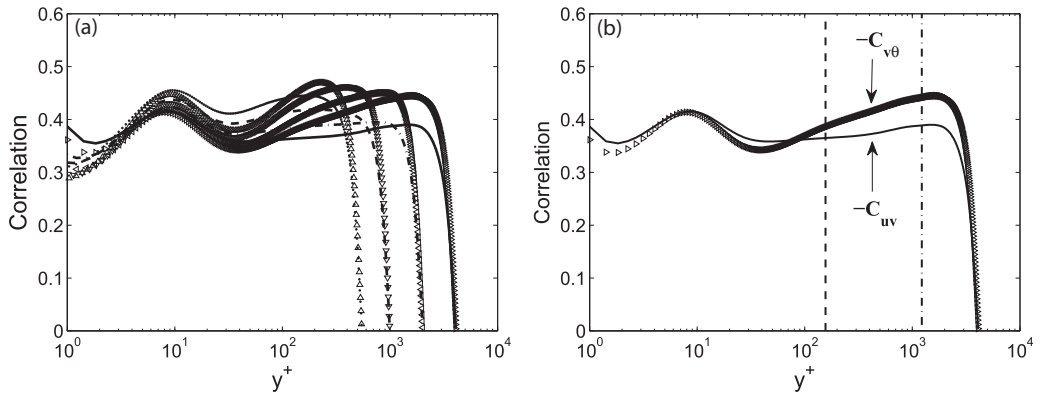

FIG. 8. (a) Profiles of correlation coefficient. Dotted line, $-C_{uv}$, $\delta^+ = 548$; dashed line, $-C_{uv}$, $\delta^+ =$ 995; dashed-dotted line, $-C_{uv}$, $\delta^+ = 2017$; solid line, $-C_{uv}$, $\delta^+ = 4088$; $\bigtriangleup$, $-C_{v\theta}$, $\delta^+ = 548$, Pr $= 1$; $\bigtriangledown$, $-C_{v\theta}$, $\delta^+ = 995$, Pr $= 1$; $\triangleleft$, $-C_{v\theta}$, $\delta^+ = 2017$, Pr $= 1$; $\triangleright$, $-C_{v\theta}$, $\delta^+ = 4088$, Pr $= 1$. (b) Profiles of correlation coefficient. Solid line, $-C_{uv}$, $\delta^+ = 4088$; $\triangleright$, $-C_{v\theta}$, $\delta^+ = 4088$, Pr $= 1$. The vertical dashed line denotes the external bound of layer III for mean scalar balance. The vertical dashed-dotted line denotes $y^+ = 0.3\delta^+$.

As discussed relative to Fig. 7, we reiterate that the streamwise velocity, u, and the wall-normal velocity, v, are related to each other through continuity. The correlation coefficient profiles indicate, however, that the unconstrained θ is more linearly correlated with v than is u. This phenomenon apparently leads to the observation that the continuity constraints on u and v render them less linearly correlated in this region of the flow. These effects are associated with the subtle variations in $T^+(y^+)$ and $T_\theta^+(y^+)$ (for $\mathrm{Pr} = 1$) observed in Fig. 6(b), and as revealed in Fig. 7 apparently arise from differences in the change of scale effects on dT^+/dy^+ and dT_θ^+/dy^+. These underlie the modifications to the scaling layer hierarchies associated with the logarithmic profile solutions on the inertial domain.

IV. CONCLUSIONS AND DISCUSSION

Properties of the layer structure associated with total scalar variance equation in fully developed turbulent channel flow with uniform scalar generation are revealed and investigated. These properties were explored using the DNS data sets of Pirozzoli *et al.* [18], which cover $548 \lesssim \delta^+ \lesssim 4088$ and $0.2 \lesssim \mathrm{Pr} \lesssim 1$. Quantitatively, the layer thicknesses are found to exhibit distinct Reynolds number and Prandtl number dependencies. Similar to the total kinetic energy equation, a four-layer structure is revealed. As is evident, the width of the layer closest to the wall (layer i) is characterized by a thermal inner scale, $\sqrt{\nu^2\alpha/u_\tau^3\delta}$, which leads the inner-normalized thickness of this layer to scale with $1/\sqrt{\mathrm{Pr}\delta^+}$. Analytical results indicate that the layer iii width follows a $(\delta^+ - \sqrt{\delta^+/\mathrm{Pr}})$ dependence at finite Reynolds numbers for each fixed Prandtl number. This finding is supported by the data. Quantitatively, the present results indicate that the layer scaling behaviors associated with the scalar variance differ substantially from those of the total kinetic energy balance and the mean scalar balance.

Previous empirically and analytically based estimates by Pirozzoli *et al.* [18] and by Zhou *et al.* [8], respectively, indicated the value of scalar Kármán constant. They both found that k_θ is greater than the Kármán constant, k, for momentum. The analytical finding is based on the properties of the similarity solution for the logarithmic mean profile over the inertial (nondiffusive) domain. For $\mathrm{Pr} = 1$, the two formulations yield the same differential equation with the same boundary conditions. Given this, the present framework provides a clear basis for evaluating the origins of the noted difference. Consistent with the previous observations of Pirozzoli *et al.* [18], the present analyses indicate that the pressure-strain term in the streamwise velocity budget equation that is absent in the scalar budget equation plays a significant role. Investigation of the Reynolds sear stress and turbulent heat flux shows the scalar θ is more linearly correlated with v than streamwise velocity u over the inertial (nondiffusive) domain, even if the development of the u is more constrained by v due to incompressibility. Within the context of the present theory, these effects lead to a modification of an internal scaling layer hierarchy via subtle difference between the Reynolds stress and turbulent heat flux gradients. This changes the exact distance from the wall scaling attained in the scalar versus momentum formulations, and thus the slope of the respective logarithmic mean profiles.

ACKNOWLEDGMENTS

A.Z. and J.K. gratefully acknowledge the support from the Australian Research Council (Grant No. DP150102593). S.P. wishes to acknowledge the PRACE Research Infrastructure resource MARCONI based at CINECA (Casalecchio di Reno, Italy) for providing the computational resources.

[1] A. Izakson, On the formula for the velocity distribution near walls, Tech. Phys. USSR IV **2**, 155 (1937).

[2] C. B. Millikan, A critical discussion of turbulent flows in channels and circular tubes, in *Proc. 5th Intl. Cong. Appl. Mech.* (Cambridge, MA, 1938), pp. 386–392.

[3] H. Tennekes and J. L. Lumley, *A First Course in Turbulence* (MIT Press, Cambridge, MA, 1972).
[4] B. A. Kader, Heat and mass transfer in pressure-gradient boundary layers, Int. J. Heat Mass Transfer **34**, 2837 (1991).
[5] T. Wei, P. Fife, J. Klewicki, and P. McMurtry, Properties of the mean momentum balance in turbulent boundary layer, pipe and channel flows, J. Fluid Mech. **522**, 303 (2005).
[6] T. Wei, P. Fife, J. Klewicki, and P. McMurtry, Scaling heat transfer in fully developed turbulent channel flow, Int. J. Heat Mass Transfer **48**, 5284 (2005).
[7] S. Saha, J. Klewicki, A. Ooi, H. Blackburn, and T. Wei, Scaling properties of the equation for passive scalar transport in wall-bounded turbulent flows, Int. J. Heat Mass Transfer **70**, 779 (2014).
[8] A. Zhou, S. Pirozzoli, and J. Klewicki, Mean equation based scaling analysis of fully-developed turbulent channel flow with uniform heat generation, Int. J. Heat Mass Transfer **115**, 50 (2017).
[9] J. C. Klewicki, Self-similar mean dynamics in turbulent wall flows, J. Fluid Mech. **718**, 596 (2013).
[10] J. Klewicki, J. Philip, I. Marusic, K. Chauhan, and C. Morrill-Winter, Self-similarity in the inertial region of wall turbulence, Phys. Rev. E **90**, 063015 (2014).
[11] J. Klewicki and M. Oberlack, Finite Reynolds number properties of a turbulent channel flow similarity solution, Phys. Fluids **27**, 095110 (2015).
[12] A. Zhou and J. Klewicki, Properties of the streamwise velocity fluctuations in the inertial layer of turbulent boundary layers and their connection to self-similar mean dynamics, Int. J. Heat Fluid Flow **51**, 372 (2015).
[13] A. Zhou, Self-similar properties and leading balance scaling structure of wall-bounded turbulent flows, Doctoral Dissertations, University of New Hampshire, 2297 (2017).
[14] J. C. Klewicki, C. T. Morrill-Winter, and A. Zhou, Inertial logarithmic layer properties and self-similar mean dynamics, *International Symposium on Turbulence and Shear Flow Phenomena (TSFP-9)* (University of Melbourne, Melbourne, Australia, 2015), p. 3A-4.
[15] I. Marusic, J. P. Monty, M. Hultmark, and A. J. Smits, On the logarithmic region in wall turbulence, J. Fluid Mech. **716**, R3 (2013).
[16] A. Townsend, *The Structure of Turbulent Shear Flow* (Cambridge University Press, Cambridge, 1980).
[17] A. Zhou and J. Klewicki, Properties of the kinetic energy budgets in wall-bounded turbulent flows, Phys. Rev. Fluids **1**, 044408 (2016).
[18] S. Pirozzoli, M. Bernardini, and P. Orlandi, Passive scalars in turbulent channel flow at high Reynolds number, J. Fluid Mech. **788**, 614 (2016).
[19] J. Klewicki, P. Fife, and T. Wei, On the logarithmic mean profile, J. Fluid Mech. **638**, 73 (2009).
[20] C. Chin, J. Philip, J. Klewicki, A. Ooi, and I. Marusic, Reynolds-number-dependent turbulent inertia and onset of log region in pipe flows, J. Fluid Mech. **757**, 747 (2014).
[21] H. Kawamura, H. Abe, and Y. Matsuo, DNS of turbulent heat transfer in channel flow with respect to Reynolds and Prandtl number effects, Int. J. Heat Fluid Flow **20**, 196 (1999).
[22] H. Abe, H. Kawamura, and Y. Matsuo, Surface heat-flux fluctuations in a turbulent channel flow up to $\mathrm{Re}_\tau = 1020$ with $\mathrm{Pr} = 0.025$ and 0.71, Int. J. Heat Fluid Flow **25**, 404 (2004).
[23] P. J. A. Priyadarshana and J. C. Klewicki, Study of the motions contributing to the Reynolds stress in high and low Reynolds number turbulent boundary layers, Phys. Fluids **16**, 4586 (2004).